Journal of Neuroscience Methods 189 (2010) 14–22

Contents lists available at ScienceDirect

Journal of Neuroscience Methods

journal homepage: www.elsevier.com/locate/jneumeth

A self-referencing glutamate biosensor for measuring real time neuronal glutamate flux

E.S. McLamore[a,b,e,f], S. Mohanty[c,f], J. Shi[c,f], J. Claussen[a,e,f], S.S. Jedlicka[g], J.L. Rickus[a,c,e,f], D.M. Porterfield[a,c,d,e,f,*]

[a] Department of Agricultural & Biological Engineering, Purdue University, West Lafayette, IN, United States
[b] School of Civil Engineering, Purdue University, West Lafayette, IN, United States
[c] Weldon School of Biomedical Engineering, Purdue University, West Lafayette, IN, United States
[d] Department of Horticulture & Landscape Architecture, Purdue University, West Lafayette, IN, United States
[e] Birck Nanotechnology Center, Discovery Park, Purdue, United States
[f] Bindley Bioscience Center, Physiological Sensing Facility, Discovery Park, Purdue University, 1203W. State Street, West Lafayette, IN, 47907-2057, United States
[g] Department of Materials Science and Engineering, Lehigh University, United States

ARTICLE INFO

Article history:
Received 9 November 2009
Received in revised form 14 January 2010
Accepted 2 March 2010

Keywords:
Glutamate
Self-referencing
Biosensor
Flux
Transport

ABSTRACT

Quantification of neurotransmitter transport dynamics is hindered by a lack of sufficient tools to directly monitor bioactive flux under physiological conditions. Traditional techniques for studying neurotransmitter release/uptake require inferences from non-selective electrical recordings, are invasive/destructive, and/or suffer from poor temporal resolution. Recent advances in electrochemical biosensors have enhanced in vitro and in vivo detection of neurotransmitter concentration under physiological/pathophysiological conditions. The use of enzymatic biosensors with performance enhancing materials (e.g., carbon nanotubes) has been a major focus for many of these advances. However, these techniques are not used as mainstream neuroscience research tools, due to relatively low sensitivity, excessive drift/noise, low signal-to-noise ratio, and inability to quantify rapid neurochemical kinetics during synaptic transmission. A sensing technique known as self-referencing overcomes many of these problems, and allows non-invasive quantification of biophysical transport. This work presents a self-referencing CNT modified glutamate oxidase biosensor for monitoring glutamate flux near neural/neuronal cells. Concentration of basal glutamate was similar to other in vivo and in vitro measurements. The biosensor was used in self-referencing (oscillating) mode to measure net glutamate flux near neural cells during electrical stimulation. Prior to stimulation, the average influx was $33.9 \pm 6.4\,\text{fmol}\,\text{cm}^{-2}\,\text{s}^{-1}$). Glutamate efflux took place immediately following stimulation, and was always followed by uptake in the 50–150 $\text{fmol}\,\text{cm}^{-2}\,\text{s}^{-1}$ range. Uptake was inhibited using threo-β-benzyloxyaspartate, and average surface flux in replicate cells ($1.1 \pm 7.4\,\text{fmol}\,\text{cm}^{-2}\,\text{s}^{-1}$) was significantly lower than uninhibited cells. The technique is extremely valuable for studying neuropathological conditions related to neurotransmission under dynamic physiological conditions.

1. Introduction

Glutamate (Glu) is an important excitatory neurotransmitter and gliotransmitter in the central nervous system. The modulation of extracellular Glu by the dynamic release and uptake from neurons and astrocytes is a primary mechanism for neural communication (Nedergaard et al., 2002; Bushong et al., 2002; Danbolt, 2001). Dynamics of glutamatergic excitation play a vital role in normal physiological processes including synaptic plasticity, differentiation, apoptosis, and long-term potentiation (Tabuchi et al., 1996; Haydon, 2001; Tapiero et al., 2002; Holden, 2003; Perea and Araque, 2007; Perea et al., 2009). In addition, abnormalities in Glu transport are associated with many illnesses, including schizophrenia, amyotrophic lateral sclerosis, epilepsy, Parkinson's disease, and cerebral ischemia (Nakanishi, 1992; Ye et al., 1999; Cid et al., 2003; Mueller et al., 2004; Ouyang et al., 2007; Krivoy et al., 2008; Staats and van Den Bosch, 2009; Ni and Púrpura, 2009; Crino, 2009; Schmitz et al., 2009). High Glu concentrations in the neural environment induce excitotoxicity through receptor activation and calcium-mediated processes, which can trigger neuronal degeneration and cell death (Chang and Lowenstein, 2003; Gagliardi, 2000; Matute et al., 2007). Highly sensitive, non-invasive techniques for quantifying dynamic changes in Glu release and uptake are needed

* Corresponding author at: Department of Agricultural & Biological Engineering, Purdue University, West Lafayette, IN 47906, United States. Tel.: +1 765 494 1197.
E-mail address: porterf@purdue.edu (D.M. Porterfield).

0165-0270/$ – see front matter © 2010 Elsevier B.V. All rights reserved.
doi:10.1016/j.jneumeth.2010.03.001

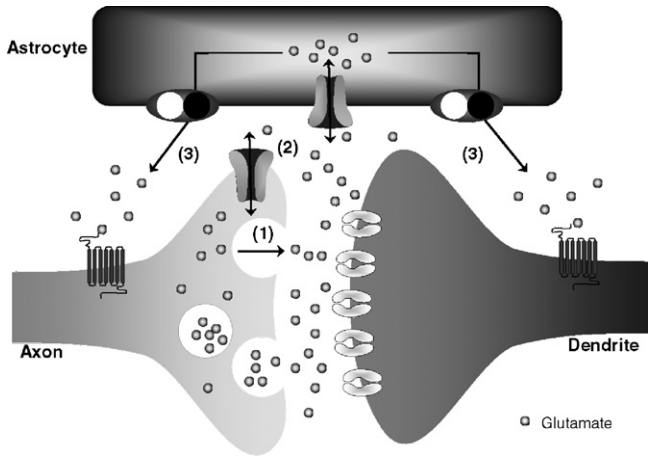

Fig. 1. Simplified representation of glutamate cycling in the tripartite synapse showing primary mechanisms of glutamate release and uptake. (1) Ca^{2+} dependent vesicular glutamate release, (2) neuronal and astrocytic uptake and reversal of glutamate transporters, (3) Ca^{2+} dependent astrocytic glutamate release.

to enhance our understanding of the complex neurochemistry associated with neurotransmission.

Fig. 1 illustrates the sources and sinks of extracellular Glu at a simplified tripartite synapse formed by pre- and post-synaptic neurons and neighboring astrocytes. Net Glu transport is comprised of neurotransmission (millisecond temporal domain), and astrocytic uptake/release (tens of seconds) (Perea et al., 2009; Pin and Duvoisin, 1995). Neuronal Glu release typically occurs by Ca^{2+} dependent vesicular release (Allen and Barres, 2009; Kaupmann et al., 1997), although certain conditions can also lead to the Ca^{2+} independent reversal of Glu transporters (Rossi et al., 2000). Astrocytes release Glu by several different possible Ca^{2+} dependent and Ca^{2+} independent mechanisms including: regulated exocitosis (Ni et al., 2007; Halassa et al., 2006), reversal of plasma membrane transporters (Szatkowski, 1990), volume sensitive anionic channels (Takano et al., 2005), and gap junction hemichannels (Ye et al., 2003). Uptake of extracellular Glu occurs in both neurons and astrocytes via excitatory amino acid transporters (EAATs) (Bergles and Jahr, 1997; Perea et al., 2009). EAATs are electrogenic exchangers that co-transport sodium with Glu and exchange potassium (Wu and Fujikawa, 2002). Uptake by EAATs is the primary mechanism by which extracellular Glu is cleared during synaptic transmission (Allen and Barres, 2009).

A number of techniques are available for measuring Glu concentration, including optical methods (Rickus et al., 2001), patch clamp (Copenhagen and Jahr, 1989; Hume et al., 1983), and microdialysis (Chen and Lunte, 1995). Nearly all of these techniques suffer from disadvantages, including: invasive sampling, temporal limitations, low signal-to-noise ratio, lack of economical feasibility, and/or ability to detect changes in Glu transport under physiological conditions. These disadvantages limit the applicability of results regarding neurotransmitter kinetics. Analytical methods such as high performance liquid chromatography and gas chromatography/mass spectrometry (Jedlicka et al., 2009) and coupled techniques (e.g., microdialysis) are capable of quantifying Glu concentrations under physiological conditions (Watson et al., 2006), but cannot measure dynamic Glu flux, and are temporally constrained (due to bulk sampling) (Day et al., 2006). Thus, real-time autonomous techniques, which are capable of providing non-invasive quantification of Glu transport dynamics in neuronal cultures, are needed. In particular, techniques which, have the ability to quantify magnitude *and* direction of Glu transport in the neural environment, are desired.

Electrochemical microelectrodes resolve some disadvantages previously listed, and can successfully measure Glu concentration near cultured cells (Niwa et al., 1997), hippocampal slices (Oldenziel et al., 2007), and *in vivo* in rats (Burmeister and Gerhardt, 2001; Day et al., 2006). Amperometric transduction techniques are most commonly used for electrochemical detection of neurotransmitters (e.g., glutamate, serotonin and nitric oxide) (Dale et al., 2005; Wilson and Gifford, 2005). The use of carbon nanotubes (CNT) and nanopatterned metals such as platinum have been shown to increase electron transfer (and therefore sensitivity) in microelectrodes (Hrapovic et al., 2004; Gong et al., 2005; Chang et al., 2007). Selectivity of amperometric sensors is greatly enhanced by the use of enzymatic recognition elements (Kauffman, 2003). Enzymes (e.g., glutamate oxidase) are immobilized on highly conductive metal surfaces (e.g., platinum), with electron flow measured via oxidative amperometry (Porterfield, 2007; ul Haque et al., 2007).

Used under standard operation, there are numerous limitations to monitoring analyte concentration at the surface of biological cells/tissues using microelectrodes. These limitations include a relatively large signal-to-noise ratio, drift and noise, and an inability to directly quantify direction of Glu flux. When using sensors in the concentration domain, small changes in measured signals associated with physiological transport (commonly in the nV range) are lost to background noise (commonly in the μV range). Due to these limitations, researchers have developed a non-invasive sensing technique, which extends and enhances the data recorded by concentration mode sensors known as the self-referencing (SR) technique (Jaffe and Nuccitelli, 1974; Borgens, 1984; Porterfield, 2007). The SR technique is a phase sensitive sensing modality based on Fick's first law of diffusion (Eq. (1)), where a microsensor is oscillated between two positions using computer-controlled stepper motors. If change in analyte concentration (ΔC) is continuously recorded at two positions separated by a fixed excursion distance (ΔX), real time measurement of flux may be obtained (Jaffe and Nuccitelli, 1974).

$$J = -D\frac{\Delta C}{\Delta X} \quad (1)$$

where J is the analyte flux and D is the molecular diffusion coefficient. Multi-dimensional SR analysis has been conducted (Kunkel et al., 2006), although these studies have a reduced temporal resolution (12–30 s). In addition, one-dimensional analysis is sufficient for describing surface transport to/from cells, monolayers, tissues; because the majority of active biological transport near a cell/tissue surface occurs in the direction perpendicular to the tangent of the surface. Based on this biophysical principle, transport within the unstirred layer can be described by one-dimensional Fickian diffusion, and if a sensor is oscillated near a cell/tissue surface at a frequency that avoids stirring, biophysical flux is directly quantified (Jaffe and Nuccitelli, 1974). The term biophysical flux denotes that measured gradients are the direct result of membrane transport activity; not passive diffusive gradient flux (Porterfield, 2007). As opposed to monitoring static concentration at the surface of cells/tissues using traditional sensing techniques, direct monitoring of biophysical flux ($J = C \cdot v$) provides dynamic information about the direction, or velocity (v) and magnitude (C) of Glu transport.

The improvement in signal-to-noise ratio when using the SR technique is due to phase sensitive detection within the unstirred layer near cell/tissue surfaces. Using a single sensor, drift and noise at each measurement position are in phase (Porterfield, 2007), and as long as the sensor is oscillated within the portion of the mass boundary layer (MBL), which can be described using a linear model (first order Fickian diffusion), extraneous noise and drift cancel upon calculation of flux. This reduction in noise is highly beneficial in describing physiological transport, and has many

advantages over traditional microsensor analyses. Among these are improved signal-to-noise ratio, reduced drift/noise, and lack of complex mathematical modeling requiring many assumptions (Jaffe and Nuccitelli, 1974; Porterfield, 2007). SR has been used to non-invasively quantify real time transport in the cellular to whole tissue domain, and has been used to enhance our understanding of dynamic physiological transport in many fields (Porterfield, 2007), including: neurobiology (Land et al., 1999), plant physiology (Gilliham et al., 2006), developmental biology (Porterfield et al., 1998), spinal cord damage (Borgens, 1984; Zuberi et al., 2008), ecotoxicology (Sanchez et al., 2008), and microbial biofilm physiology (McLamore et al., 2009).

In this study, we develop a novel highly sensitive/selective enzyme based micro-biosensor for measuring Glu. The biosensor was used in the SR modality for direct non-invasive quantification of Glu flux from neural/neuronal cells (neurons, astrocytes, and oligodendrocytes). Use of the highly sensitive noise filtering SR technique was coupled with a pharmacological inhibition study to improve our understanding of spatially and temporally dynamic Glu transport in neuronal cells.

2. Methodology

2.1. Cell culture

Mouse derived P19 cells (CRL-1825) (American Type Culture Collection (ATCC); Manassas, VA) (McBurney and Rogers, 1982) were grown in α-MEM (Mediatech, Manassas, VA) supplemented with 7.5% bovine calf serum (BCS) and 2.5% fetal bovine serum (FBS) (Hyclone, Waltham, MA). Cultures were passaged at 75% confluency using trypsin (Hyclone, Waltham, MA) and maintained as a monolayer. Differentiation was induced using 5×10^{-7} M all-trans retinoic acid (Sigma Aldrich, St. Louis, MO) and α-MEM media supplemented with 0.5% FBS. Cells were treated with retinoic acid for 4 days in non-adherent condition causing cells to differentiate into neurons, astrocytes, oligodendrocytes, and fibroblast-like cells (Jones-Villeneuve et al., 1982, 1983). After retinoic acid treatment, differentiated cells were plated at a density of 4×10^4 cells/cm^2 on UV treated culture dishes coated with 0.5 mg/mL rat tail collagen (BD Biosciences, Franklin Lakes, NJ), and allowed to mature for 10–14 days. Under these conditions, approximately 16% of the cells are neurons and 7% are astrocytes (Jedlicka et al., 2007). Differentiated P19 cells respond to electrical stimulation by release of both Glu and GABA (Jedlicka et al., 2009).

2.2. Biosensor construction

Microelectrodes were constructed from 2 to 5 μm tip diameter platinum/iridium wires insulated with parylene (Microprobe Inc., Gaithersburg, MD). Microelectrodes were cleaned thoroughly with DI water, ultrasonicated, and cleaned via cyclic voltammetry using a Bioanalytical Systems (BASi) C3 Cell Stand (West Lafayette, IN) with 1.0 M sulfuric acid to remove any impurities (scan rate was 40 mV/s). The functional surface area was then electroplated with platinum black (mesoporous platinum) using a bare platinum wire as a counter electrode during electrodeposition at 10 V for 40 s in 0.72% (*v*/*v*) hexochloroplatinate (Sigma Aldrich, St. Louis, MO) and 0.0001% (*v*/*v*) lead acetate. Platinized microelectrodes were dip-coated in a solution of multiwalled carbon nanotubes (MWCNT; Cheap Tubes, Inc., Battleboro, Vermont) suspended in Nafion (Sigma–Aldrich, St. Louis, MO) at a concentration of 2 mg/mL. MWCNT/Nafion coated electrodes were then biofunctionalized by dip coating in a mixture of 1% bovine serum albumin (Sigma–Aldrich, St. Louis, MO), 0.125% glutaraldehyde (Sigma–Aldrich, St. Louis, MO), and 1% glutamate oxidase (GluOx, EC 1.4.3.11; Seikagaku Inc., Abingdon, UK). Oxidative amperometry was used to detect H_2O_2 produced by the oxidation of Glu by GluOx at a polarization potential of +700 mV according to Eq. (2) (Day et al., 2006). Fabricated electrodes were stored at +4 °C for up to 14 days, and stability reported as a percent change in sensitivity.

$$\text{glutamate} + H_2O \xrightarrow{\text{glutamate oxidase}} \alpha\text{-ketoglutarate} + H_2O_2 \quad (2)$$

2.3. Imaging

Field emission scanning electron microscopy (FESEM) micrographs of the MWCNT/Nafion biosensor functional tip were obtained by a Hitachi S-4800 microscope at a power setting of 5.0 kV and magnification of 40k. The platinized biosensor tip was dip-coated with the MWCNT/Nafion solution and allowed to dry overnight before imaging. No preprocessing was required for FESEM of the MWCNT/Nafion biosensor functional tip.

Immunofluorescence staining was conducted using techniques in Jedlicka et al. (2009). Differentiated P19 cells were fixed using 4% paraformaldehyde (10 min), washed in PBS, and cells were then permeabilized with 0.1% Triton X-100. Primary antibodies (β-tubulin III (AbCam)) were incubated overnight at 4 °C, and secondary antibodies were incubated for 1 h at 20 °C. Nuclear staining was conducted using Hoechst 33258. After the final washing, the cells were analyzed using a Bio-Rad Radiance Multiphoton confocal microscope.

2.4. Calibration

Cyclic voltammetry was performed between −800 to +800 mV at a scan rate of 20 mV/s on a BASi cell stand to characterize redox chemistry. A consistent peak at 300 mV was observed as the redox potential of the GluOx biosensor. Ten biosensors were fabricated and calibrated a minimum of three times. Fabricated biosensors were first tested for selectivity towards hydrogen peroxide (Sigma–Aldrich) in the 1–100 μM range using a BASi cell stand at +700 mV vs. a Ag/AgCl reference electrode (3 M KCl). Biosensors were then calibrated in PBS (pH = 7) using L-glutamic acid (Sigma–Aldrich) concentrations ranging from 0.1 to 100 μM. The slopes of the concentration vs. current plots at +700 mV polarization potential were plotted, and linear regression used to characterize the slope and y-intercept for each plot. Limit of detection was calculated based on the tangential technique reported by Diamond (1998). For concentration measurements, temporal resolution (t_{95}) was calculated by averaging the 95% steady state response time over the linear range tested. During Glu sensor calibration, steady state was defined as a less than 1% change in sensor output for a minimum of 5000 current measurements at 1 kHz. The biosensor was tested for selectivity over ascorbate by comparing the electrode to Glu addition with the response to ascorbate addition within the 1–250 μM range. Selectivity results are reported as the ratio of the linear slope of the calibration curve (Glu:ascorbate).

2.5. Self-referencing operation

GluOx biosensors were tested for operation in self-referencing mode by oscillating at various frequencies in a known abiotic concentration gradient. For SR sensors to be operated within the constraints of Fick's first law of diffusion (Eq. (1)), measured changes in concentration over the excursion distance must fall within the linear portion of the curve describing the mass boundary layer (MBL). The linear range may be estimated as the distance at one half the value of the total change in concentration over the entire thickness of the MBL, which is empirically measured (Porterfield, 2007). To determine the MBL thickness and optimum oscillation distance, a 1.5-mm borosilicate glass capillary

(World Precision Instruments, Sarasota FL) was pulled on a horizontal puller (Sutter instrument Co., Novato, CA) to produce a tip diameter of 50 μm, and back filled with a heated solution containing 5 mM Glu and 0.5% agar. The filled pipette was fixed in a petri dish containing Locke's buffer and 1 μM Glu (creating a concentration gradient between the filled pipette and the bath) and the chemical gradient near the tip was allowed to stabilize for 30 min. A calibrated GluOx biosensor was mounted on a head stage controlled by a motion control system. The biosensor and a reference electrode were placed into the dish containing the filled pipette, and polarized for 20 min. The biosensor and filled pipette were adjusted to the same focal plane using a video/zoomscope (Pulnix, San Jose, CA), and the sensor was moved to within 1 μm of the pipette tip. Glu flux was measured at an oscillation frequency within the 0.20–0.50 Hz range suggested by Kühtreiber and Jaffe (1990) to avoid stirring of the unstirred boundary layer and maximize signal-to-noise ratio. The sensor was then positioned 5 μm from the pipette surface, and flux recorded (nine repetitions). This process was repeated in a step-back fashion. Results from these step back experiments were compared to first order Fickian diffusion models. The model was developed by assuming isotropic diffusion from the edge of a cylinder using empirical values of the mass boundary layer thickness (McLamore et al., 2009). The correlation coefficient between the predicted and measured flux was calculated, and is reported as the dynamic efficiency (ε).

Automated Scanning Electrode Technique (ASET) software was used for data acquisition (A/D) and control functions (D/A) (Science Wares, Falmouth, MA). The A/D board with DC-coupled differential amplifier, low/high pass filters, and video/data acquisition system were obtained through Applicable Electronics, Inc. (Sandwich, MA). All SR experiments were conducted on a vibration isolation table equipped with a Faraday cage (Technical Manufacturing Co., Peabody, MA). The overall sample rate for all SR experiments was 1 kHz.

2.6. Neural glutamate flux

All biological experiments were conducted within a 10–14 day window from the day of induction. Differentiated P19 cells were rinsed in PBS to remove cell culture medium, and incubated in 20 mL of Locke's buffer at 37 °C: 94 mM NaCl, 4.0 mM KCl, 1.0 mM $MgCl_2$, 1.8 mM $CaCl_2$, 10 mM HEPES (pH = 7.4), and 5.0 mM glucose. Real time Glu flux was recorded at the surface (within 1 μm) of cell clusters during induced depolarization using 150 μL injections of Locke's buffer with a relatively high potassium concentration (53 mM KCl; 400 nM incremental additions of K^+). A syringe pump was used to inject the high-potassium Locke's buffer to limit mechanical noise due to convection. To ensure that the recorded spikes were not caused by convection or the added potassium on the biosensor itself (false positive), flux was measured at the surface of a pipette filled with 5 mM glutamate and 0.5% agar in Locke's buffer, and 150 μL additions of Locke's buffer with 53 mM potassium chloride were injected (zero control).

Pharmacological studies were used in an attempt to understand physiological Glu transport by neuron/neural cells (Hu et al., 1994; Day et al., 2006). Threo-β-benzyloxyaspartate (TBOA), an inhibitor of Glu uptake (Jabaudon et al., 1999), was injected into the culture dish immediately following PBS rinsing and allowed to rest for 30 min prior to recording of flux measurements (preliminary experiments indicated 30 min was sufficient for inhibition of EAAT). Zero control experiments were conducted using an abiotic diffusion source as previously described in the presence of 100 μM TBOA to ensure sensor output was not affected by TBOA addition.

Glu uptake kinetics were empirically modeled for each electrophysiological stimulation using a three parameter exponential decay model. Average data represent six successive stimulations for three replicate plates (18 total events analyzed). All error bars represent ±2S.E. of the arithmetic mean (n values are provided). Where applicable, statistical analyses were conducted using either a Students t-test, or analysis of variance (ANOVA). In each case, an α value of 0.05 was used and p-values reported.

3. Results and discussion

3.1. Biosensor calibration

Performance of platinized, MWCNT/Nafion GluOx microbiosensors ($n = 7$) was similar to other microsensor designs reported in the literature (Day et al., 2006). Sensitivity to H_2O_2 in PBS (pH = 7.4) was 0.9 ± 0.3 nA μM^{-1} for peroxide concentrations up to 100 μM. When operated in a three-electrode scheme (working, reference and auxiliary electrode), sensitivity to Glu was 0.5 nA μM^{-1}. However, all self-referencing experiments were conducted in a two-electrode scheme (working and reference electrode), with a working sensitivity was 46.6 pA μM^{-1}. Temporal resolution (t_{95}) during calibration was 1.1 ± 0.3 s within the range tested, which is similar to other enzyme biosensor techniques (Day et al., 2006).

Fig. 2 presents the lower end of the linear range, although calibration plots were linear up to Glu concentrations of 100 μM (see supplemental Fig. S1). The limit of detection was 0.9 ± 0.3 μM ($n = 7$), and the measured sensitivity per electrode active surface area was 473 ± 57 μA μM^{-1} cm^{-2}. The limit of detection and dynamic range (0–130 μM) covered expected extracellular Glu concentrations measured in brain tissue (1–5 μM) estimated using microdialysis (Baker et al., 2002; Zhang et al., 2005). Selectivity over ascorbate (ratio of linear slopes was 275:1; glutamate:ascorbate) was a significant improvement relative to previously reported values (Day et al., 2006). This improvement is hypothesized to be due to the enhanced electron transfer by the combination of amorphous nanopatterned platinum and CNT layers (Wang et al., 2003; Hrapovic et al., 2004). Sensor stability was at least 14 days when stored at room temperature (less than 5% change in sensitivity).

A calibrated GluOx biosensor was validated for use as a self-referencing flux sensor in a known concentration gradient (Fig. 2). The oscillation frequency was 0.33 Hz and the excursion distance was 30 μm. For SR analysis, the temporal resolution was 1.5 s, and was equal to one half the oscillation period based on the algorithm in McLamore et al. (2009). The one-dimensional diffusion model was developed based on McLamore et al. (2009), and the dynamic efficiency of the sensor was 0.98. For all SR GluOx biosensors, the ΔX value (30 μm) was well within the measured linear distance (235 μm), validating the use of Fick's first law of diffusion.

3.2. Neural glutamate flux

Following calibration and validation under abiotic conditions, a SR GluOx biosensor was positioned 1 μm above the surface of the cells using computer-controlled stepper motors. Using optical imaging, neurons, astrocytes, and neural processes were easily identified by their morphology (Jedlicka et al., 2009). Fig. 3 depicts the size of the biosensor tip relative to a neuron. Glutamate transport occurs within the nanoscale spatial domain with a temporal resolution of ~ms (synaptic) to tens of seconds (astrocytic) (Perea et al., 2009). Therefore, self-referencing GluOx biosensors are unlikely to resolve single synaptic release/uptake, but rather quantify net Glu transport in the extrasynaptic space in the direction of sensor oscillation.

To demonstrate the ability of the self-referencing GluOx biosensor to quantify biophysical flux, 225 μM (500 μL) Glu was added to the culture dish containing Locke's buffer, and the oscillating sen-

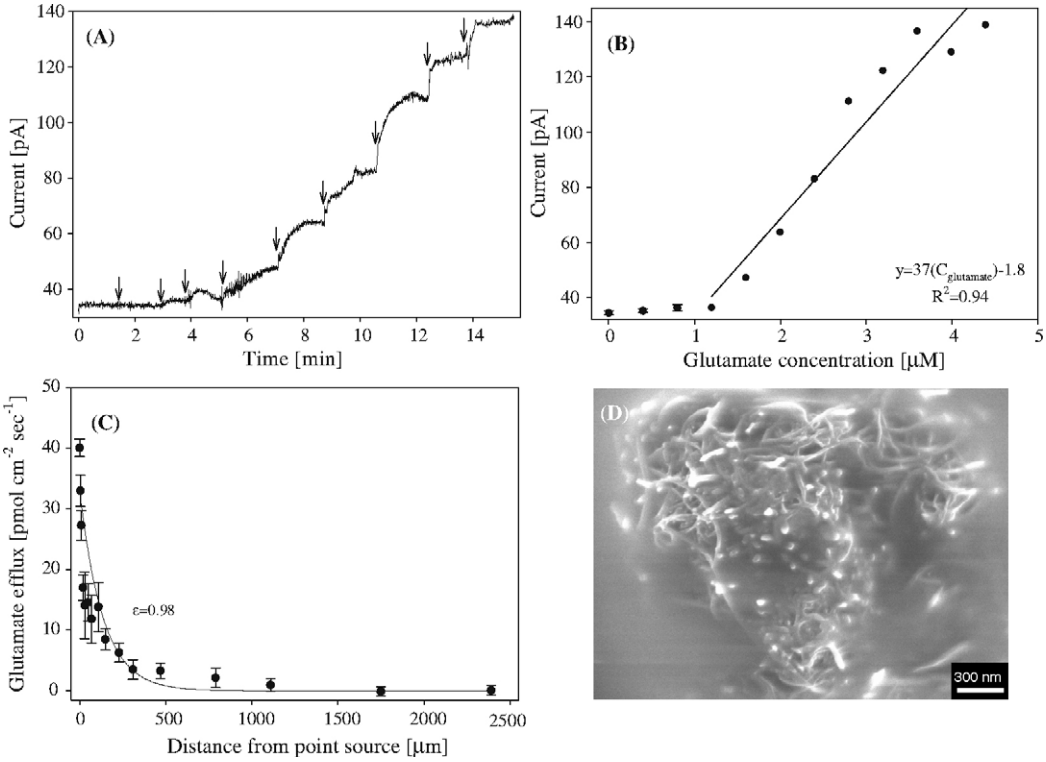

Fig. 2. (A) Amperometric calibration of GluOx biosensor in Locke's buffer (pH = 7.4) at a polarization potential of +700 mV. Arrows indicate the addition of glutamate. (B) Average steady state current as a function of glutamate concentration The $R^2 = 0.97$ for linear range of operation ($n = 1000$ current readings for each step). (C) Step back experiment from a pipette filled with 5 mM glutamate and 0.5% agar in Locke's buffer (pH = 7.4) with 1 μM glutamate (dynamic efficiency was 0.98) ($n = 12$ measurement cycles at each position). (D) Field emission scanning electron microscopy micrograph of MWCNT/Nafion/GluOx biosensor functional tip.

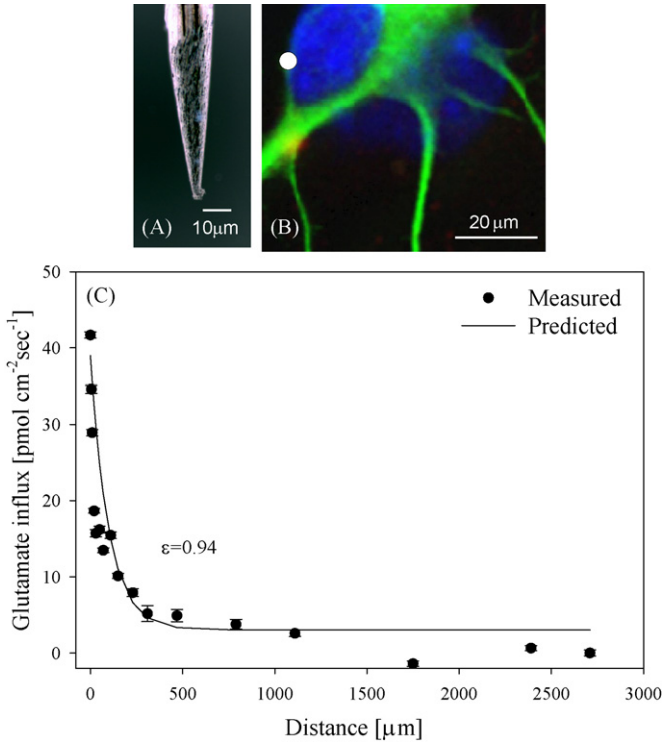

Fig. 3. (A) Light microscope image of the GluOx biosensor. (B) Immunochemical fluorescent micrograph of P19 differentiated neuron (green: β-tubulin III (Tuj1+), blue: nuclei (Hoechst 33258)); white dot indicates size of biosensor tip. (C) Step back experiment from mixed population neuronal cells following external addition of 225 μM glutamic acid. Oscillation frequency was 0.33 Hz, excursion distance was 30 μm, and dynamic efficiency was 0.94 ($n = 12$ measurement cycles at each position).

sor (0.33 Hz) was positioned 1 μm above a cell surface and flux was recorded. The SR sensor was then progressively stepped away from the cell surface in the direction of the sensor oscillation. The surface Glu concentration following external addition of Glu was 10.6 μM (see supplemental Fig. S2). A steady influx of 41 ± 2 pmol cm^{-2} s^{-1} was measured at the surface for up to 10 min. Although this level of Glu may have induced excitotoxic effects, this experiment was used to demonstrate the ability of the SR GluOx biosensor for directly measuring biophysical transport. Predicted values were derived using a first order empirical diffusion model based on measured concentration values (McLamore et al., 2009). The self-referencing biosensor was capable of directly measuring induced Glu influx within the extracellular space ($\varepsilon = 0.94$).

Following validation of the SR GluOx biosensor for measuring active transport from a cluster of cells, Glu flux was measured 1 μm above the cells ($n = 3$). The basal extracellular Glu concentration (5.8 ± 0.6 μM) was similar to reported *in vivo* values measured using microdialysis (1–5 μM; Baker et al., 2002) and GluOx biosensors (1.4–1.8 μM; Day et al., 2006). Cells were then electrochemically stimulated with Locke's buffer containing 53 mM excess potassium to depolarize the cells and stimulate Glu release. Similar to other microelectrode measurements, an increase in extracellular Glu concentration followed by a return to basal levels occurred following stimulation (Fig. 4A). The measured increase in extracellular Glu concentration (2.1 ± 0.4 μM) was slightly lower than *in vivo* measurements (6–16 μM) measured in the striatum and frontal cortex of anesthetized rats (Day et al., 2006), although this is expected using *in vitro* measurements where the density of active cells is significantly lower than in brain tissue. This difference is also reflected in the relatively long measured rise time based on concentration measurements (1.1 ± 0.1 min). Although concentration values indicate active Glu efflux following stimulation, it is unclear from these data whether the subsequent return to basal

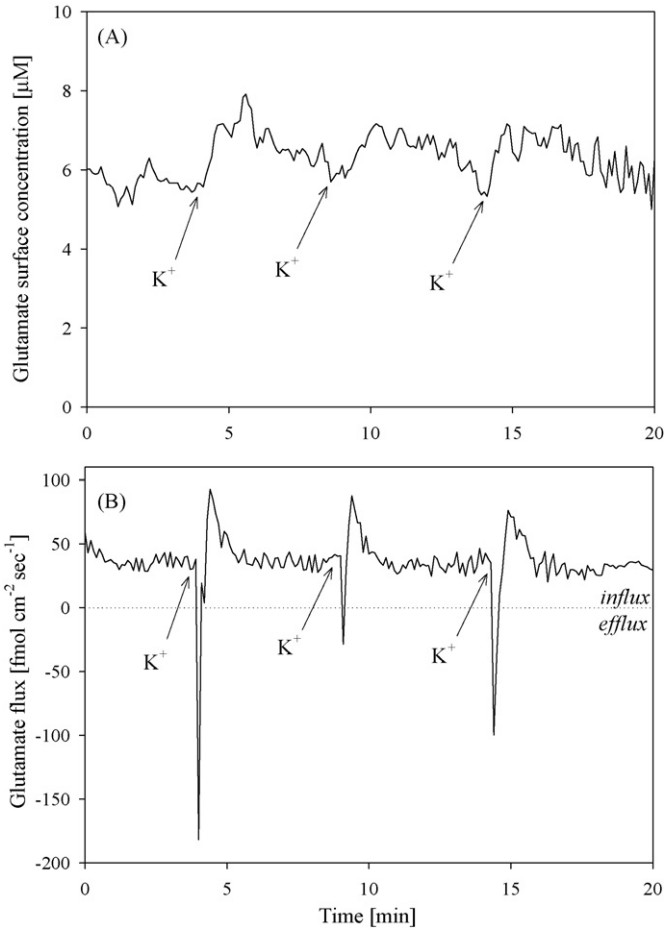

Fig. 4. (A) Glutamate surface concentration and flux (B) recorded 1 μM above the cells during three successive potassium stimulations with 150 μL of Locke's buffer containing 53 mM KCl. Increase in Glu concentration and subsequent decrease in concentration were observed following stimulation. Phase sensitive detection provided signal noise filtration required to quantify biophysical glutamate efflux and influx.

Glu concentration is due to active cellular uptake, diffusion away from the stimulation site, or a combination of the two mechanisms. The SR biosensor technique overcomes this limitation by allowing direct quantification of local Glu concentration *and* direction of transport.

Using the SR technique, significant, rapid efflux of Glu was measured, followed by subsequent uptake (Fig. 4B). In this case, efflux (negative) and influx (positive) values refer to transport that occurred in the direction perpendicular to the tangent of the cell surface. Prior to stimulation, a stable influx of Glu (33.9 ± 6.4 fmol cm^{-2} s^{-1}) was measured 1 μm above all cells measured (three independent replicates). Rapid Glu release was followed by active cellular uptake in the opposite direction of release. The ability to quantify the direction of Glu uptake following depolarization is critical, and improves our understanding of spatially and temporally dynamic Glu transport. This is a critical feature of the SR technique, as during net efflux/influx, Glu release/uptake mechanisms are both active, although during net efflux release mechanisms are more active than uptake mechanisms (and vice versa).

To test the reproducibility of the SR GluOx technique, six successive 150 μL additions of Locke's buffer with high potassium (53 mM KCl) were added to stimulate the cells. A representative plot is shown in Fig. 5, and SR data indicated that Glu efflux occurred within 1.5 ± 0.2 s, and uptake subsequently followed and lasted for an average of 1.6 ± 0.2 min. This response is consistent with rapid Glu release (~2 s) and uptake (~1 min) noted by Hu et al. (1994). Consistent with Day et al. (2006) a long (~20 min) refractory period following depolarization was not required for re-stimulation. Measurement of Glu flux at the surface of an abiotic diffusion source during addition of KCl (zero control) verified that the observed changes in Glu flux were not abiotic electrochemical effects (see supplemental Fig. S3).

Although Glu efflux following stimulation was too rapid to construct detailed models (temporal resolution when oscillating the biosensor was 1.5 s), a three parameter exponential decay model was used to fit measured re-uptake during each of the six successive simulations ($J = J_o + a \times e^{-bt}$); where: J_o =, steady state influx following stimulation (fmol cm^{-2} s^{-1}), a = peak Glu influx following stimulation (fmol cm^{-2} s^{-1}), and b = exponential uptake constant (min^{-1}). For the three replicates, the uptake kinetics were not significantly different when analyzed using ANOVA ($p = 0.046$), and the values in Fig. 5(B) represent average Glu re-uptake for all replicates ($n = 18$ stimulations) using a potassium stimulation concentration of 0.4 μM. The average exponential uptake constant for three replicates was 1.62 ± 0.05 min^{-1}.

After six successive stimulations, 10 mM KCN was added to the culture dish to block electron transport and induce cell death. Three successive additions of high-potassium Locke's buffer were again added to the culture dish, and Glu flux recorded (data not shown). Following induced cell death by KCN addition, Glu flux (0.97 ± 0.16 fmol cm^{-2} s^{-1}) was not significantly different ($p < 0.01$) from a background measurement taken 2 mm above the cell surface (1.4 ± 0.3 fmol cm^{-2} s^{-1}).

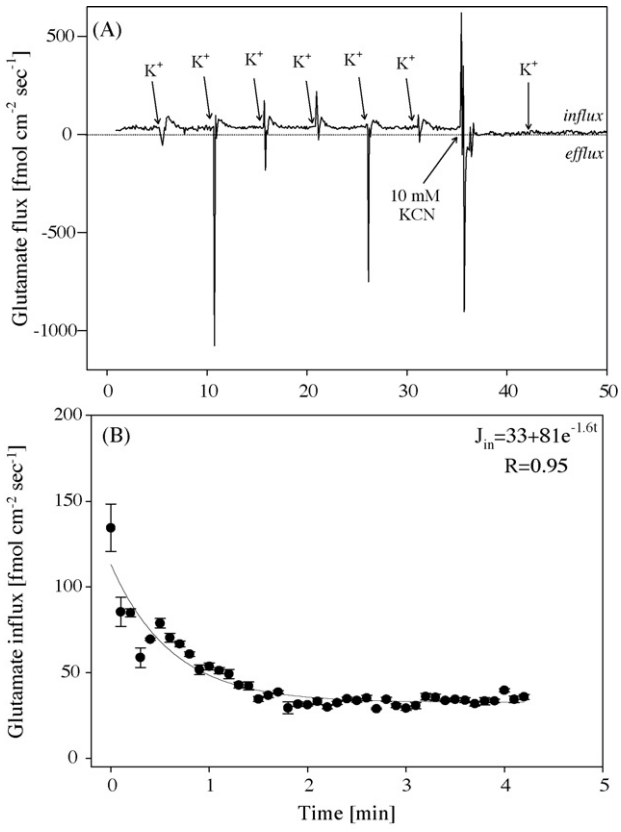

Fig. 5. (A) Stimulation of cells with 150 μL of Locke's buffer containing 53 mM KCl. After stimulation, glutamate efflux was rapid (<1.5 s), followed by uptake of glutamate. (B) Average uptake rate for all replicates ($n = 18$). An exponential decay model (three parameter) was used to fit the data, and the equation is shown. Error bars represent ±1S.E. of the arithmetic mean.

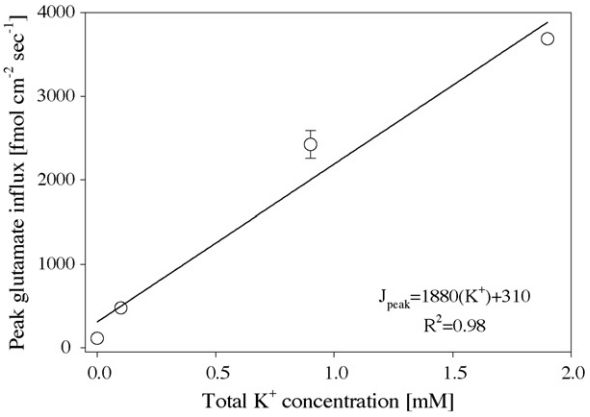

Fig. 6. Measured glutamate peak influx as a function of total concentration of added potassium. Error bars represent one SE of the arithmetic mean (n = 18).

The maximum average Glu influx for all measurements (n = 18) was plotted against the total concentration of potassium in the culture dish. The relationship between total potassium concentration and peak flux was approximated by a linear plot (Fig. 6). This potassium concentration-dependent trend was also noted using Glu concentration assays for *in vivo* measurements, although only two potassium concentrations were reported (Day et al., 2006). The consistency of the linear relationship within the range tested (R^2 = 0.97) demonstrate the ability of the phase sensitive technique to quantify Glu release.

The previous set of experiments was repeated after adding 100 μM TBOA to inhibit Glu uptake. Following 30 min the average surface glutamate concentration TBOA treated cells (7.4 ± 0.5 μM) was slightly higher than for uninhibited cells, which is consistent with results reported by Day et al. (2006). The average surface influx measured 1 μm above TBOA treated cells from three replicate plates (1.1 ± 7.4 fmol cm^{-2} s^{-1}) was not significantly different (p = 0.08) than a background measurement (1.3 ± 6.6 fmol cm^{-2} s^{-1}), but significantly lower than the flux measured from untreated cells. TBOA is an effective competitive inhibitor of glutamate uptake by all of the major EAATs. Inhibition of Glu uptake has been shown for TBOA concentrations in the 10 μM (Anderson et al., 2001) to 200 μM TBOA (Jabaudon et al., 1999) range. The IC_{50} for glutamate uptake inhibition are: EAAT1 (70 μM), EAAT2 (6 μM), and EAAT3 (6 μM) (Bonde et al., 2005; Shimamoto et al., 1998; Jabaudon et al., 1999; Waagepetersen et al., 2001). At the concentration used in this study, most neuronal and astrocytic uptake should be blocked. Indeed SR analysis indicated inhibition after as little as 30 min of exposure.

Six successive 150 μL additions of Locke's buffer with 53 mM KCl were added to each dish of TBOA treated cells, and similar efflux trends to those reported in uninhibited cells were recorded, although the peak efflux (370 ± 86 fmol cm^{-2} s^{-1}) was significantly lower than uninhibited cells (500 ± 86 fmol cm^{-2} s^{-1}); a representative plot is presented in Fig. 7). However, the peak influx (54.1 ± 1.3 fmol cm^{-2} s^{-1}) and steady state flux following stimulation (1.0 ± 0.1 fmol cm^{-2} s^{-1}) were significantly lower than uninhibited cells (p < 0.01) due to inhibition of Glu influx by TBOA. Average uptake constant (1.19 ± 0.03 min^{-1}) and kinetic values were also significantly lower for inhibited cells for all three replicates (18 total stimulations) when analyzed using ANOVA (p = 0.02). Following cell death by addition of 10 mM KCN, no significant flux values were recorded upon stimulation.

Integration of real time flux SR data provided information about net surface Glu uptake, which is a valuable parameter in understanding inherent physiology. The real time flux data in Figs. 5(A) and 7(A) were integrated for a 4-min time period

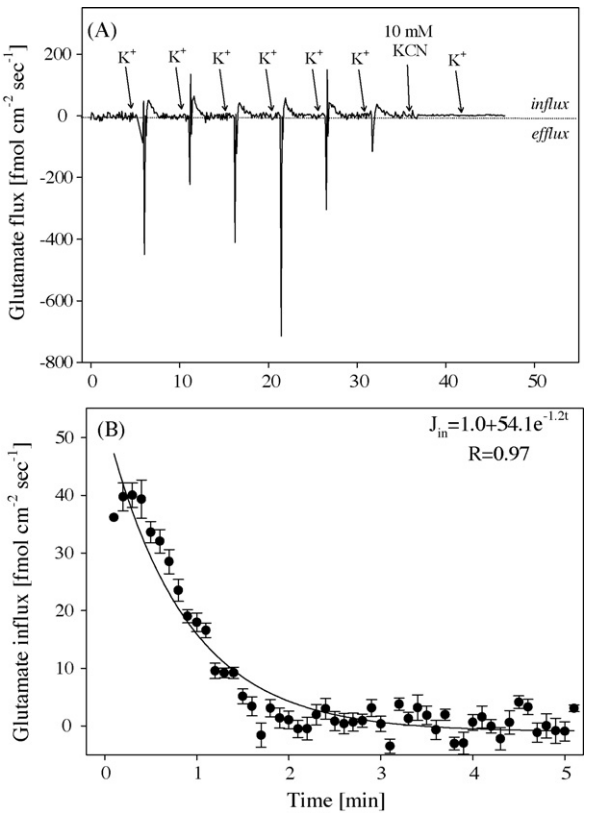

Fig. 7. (A) Potassium stimulation of neural cells following 30 min of exposure to 100 μM threo-β-benzyloxyaspartate (TBOA). (B) Average uptake rate for all replicates. An exponential decay model (three parameter) was used to fit the data, and the equation is shown. Error bars represent ±1S.E. of the arithmetic mean (n = 18).

during electrophysiological stimulation (2 min before and 2 min after stimulation), and average values plotted for all replicate experiments (n = 18). Addition of the inhibitor TBOA significantly reduced pre-stimulation and post-stimulation Glu net surface uptake (p = 0.04). Although Glu efflux following depolarization was too rapid to construct detailed models (rise time <1.5 s), integration data revealed that the average net surface release for uninhibited cells (110 ± 20 fmol cm^{-2}) was significantly larger than inhibited cells (81 ± 20 fmol cm^{-2}).

A summary of the data is presented in Table 1. As expected, the basal concentration at the surface of cells exposed to TBOA (an uptake inhibitor) was higher than uninhibited cells, which is also reflected in the basal Glu influx values (Fig. 8). Following electrophysiological potassium stimulation, the average peak influx and exponential uptake constant was significantly higher for uninhibited cells than cells exposed to TBOA. Although rapid Glu efflux was too rapid to construct detailed models, integration of real time flux data provided insight into the net Glu flux in control and uptake-inhibited cells. Before and after electrophysiological stimulation,

Table 1
Summary of glutamate flux data for uninhibited and inhibited (TBOA) cells. All averages were an average of 18 electrochemical potassium stimulations.

	Uninhibited	Inhibited
Basal Glu concentration [μm]	5.8 ± 0.6	7.4 ± 0.5
Average pre-stimulation influx [fmol cm^{-2} s^{-1}]	34 ± 6	1.1 ± 7.4
Average peak efflux [fmol cm^{-2} s^{-1}	500 ± 190	370 ± 86
Average peak influx [fmol cm^{-2} s^{-1}]	135 ± 14	36 ± 3
Average exponential uptake constant [min^{-1}]	1.62 ± 0.05	1.19 ± 0.03
Pre-stimulation iFlux [fmol cm^{-2}]	7292 ± 218	407 ± 18
Post-stimulation iFlux [fmol cm^{-2}]	11,021 ± 39	1673 ± 58

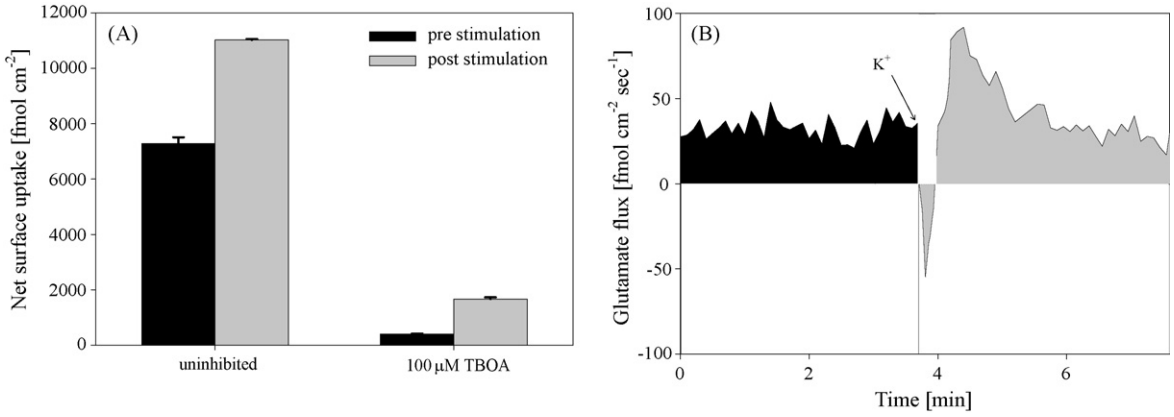

Fig. 8. (A) Net surface uptake by uninhibited neuronal cells and cells exposed to 100 μM TBOA for 30 min before and after re-uptake due to electrophysiological stimulation. Error bars represent one SE of the arithmetic mean ($n = 18$). (B) An example of a single stimulation for uninhibited cells is shown, demonstrating how integrated flux was calculated for pre-stimulation (black) and post-stimulation (gray).

the net transport in uninhibited cells was larger than inhibited cell clusters, and peak efflux was slightly higher in uninhibited clusters (validated using the integrated flux approach). As expected, peak influx and uptake rate were significantly larger in uninhibited clusters. The integrated flux technique is a novel tool, which is useful for analyzing real time data describing reversible biochemical reactions such as Glu release/uptake following stimulation. This technique is particularly useful for analyzing large sets of real time data, where multiple inhibitors with varying mode of action are utilized.

4. Conclusions

We demonstrated the use of a highly sensitive platinized MWCT/Nafion/GluOx biosensor for measuring glutamate under physiological conditions in the presence of interfering compounds (e.g., ascorbate). In self-referencing mode, this biosensor allowed direct measurement of biophysical glutamate flux from mixed neural culture (neurons, astrocytes, oligodendrocytes and fibroblasts). Glutamate release and uptake following electrophysiological stimulation with potassium were quantified using the phase sensitive technique. In addition to previous approaches, which quantified extracellular concentration, SR sensors provide additional information about the direction of active cellular transport. EAAT inhibitors blocked both post-stimulation and basal glutamate uptake indicating that the measured influx was due to classic neurotransmitter uptake mechanisms. This result demonstrates the ability of the SR GluOx biosensor for quantifying reversible and dynamic glutamate transport. The oscillating biosensor is an extremely useful tool, which has not been previously demonstrated, for understanding real time neurotransmitter dynamics in neural cells.

Acknowledgements

The authors thank Aeraj ul Haque and Alfred Diggs for support with laboratory procedures. This research was partially supported by the Office of Naval Research and the National Science Foundation.

Appendix A. Supplementary data

Supplementary data associated with this article can be found, in the online version, at doi:10.1016/j.jneumeth.2010.03.001.

References

Allen NJ, Barres BA. Glia—more than just brain glue. Nature 2009;457:675–7.
Baker DA, Xi Z, Shen H, Swanson CJ, Kalivas PW. The origin and neuronal function of in vivo nonsynaptic glutamate. J Neurosci 2002;22(20):9134–41.
Bergles DE, Jahr CE. Synaptic activation of glutamate transporters in hippocampal astrocytes. Neuron 1997;19:1297–308.
Borgens RB. Endogenous ionic currents traverse intact and damaged bone. Science 1984;225:478–82.
Burmeister JJ, Gerhardt GA. Self referencing ceramic based multisite microelectrodes for the detection and elimination of interferences from the measurement of L-glutamate and other analytes. Anal Chem 2001;73(5):1037–42.
Bushong EA, Martone ME, Jones YZ, Ellisman MH. Protoplasmic astrocytes in CA1 stratum radiatum occupy separate anatomical domains. J Neurosci 2002;22(1):183–92.
Chang BS, Lowenstein DS. Epilepsy. N Engl J Med 2003;349:1257–66.
Chang G, Oyama M, Hirao K. Platinum nano-cluster thin film formed on glassy carbon and the application for methanol oxidation. Thin Solid Films 2007;515(7–8):3311–4.
Chen A, Lunte CE. Microdialysis sampling coupled on-line to fast microbore liquid chromatography. J Chromatogr A 1995;691:29–35.
Cid C, Alvarez-Cermeno JC, Regidor I, Salinas M, Alcazar A. Low concentrations of glutamate induce apoptosis in cultured neurons: implications for amyrotrophic lateral sclerosis. J Neurol Sci 2003;206(1):91–5.
Copenhagen DR, Jahr CE. Release of endogenous excitatory amino acids from turtle photoreceptors. Nature 1989;341:536–9.
Crino PB. Focal brain malformations: seizures, signaling, sequencing. Epilepsia 2009;50:3–8.
Dale N, Hatz S, Tian F, Llaudet E. Listening to the brain: microelectrode biosensors for neurochemicals. Trends Biotechnol 2005;23:420–8.
Danbolt NC. Glutamate uptake. Prog Neurobiol 2001;65(1):1–105.
Day BK, Pomerleau F, Burmeister JJ, Huett P, Gerhardt GA. Microelectrode array studies of basal and potassium-evoked release of L-glutamate in the anesthetized rat brain. J Neurochem 2006;96:1626–35.
Diamond D. Principles of Chemical and Biological Sensors. New York, NY: John Wiley & Sons, Inc; 1998.
Gagliardi RJ. Neuroprotection, excitotoxicity and NMDA antagonists. Arquivos de Neuro-Psiquitria 2000;58:583–8.
Gilliham M, Sullivan W, Tester M, Tyerman SD. Simultaneous flux and current measurement from single plant protoplasts reveals a strong link between K^+ fluxes and current, but no link between Ca^{2+} fluxes and current. Plant J 2006;46:134–44.
Gong K, Yan Y, Meining Z, Lei S, Shaoxiang X, Lanqun M. Electrochemistry and electroanalytical applications of carbon nanotubes: a review. Anal Sci 2005;21:1383–94.
Halassa MM, Fellin T, Haydon PG. The tripartite synapse: roles for gliotransmission in health and disease. Trends Mol Med 2006;13:54–63.
Haydon PG. Glia: listening and talking to the synapse. Nat Rev Neurosci 2001;2:185–93.
Holden C. Psychiatric drugs. Excited by glutamate. Science 2003;300:1866–8.
Hrapovic S, Liu Y, Male KB, Luong JHT. Electrochemical biosensing platforms using platinum nanoparticles and carbon nanotubes. Anal Chem 2004;76(4):1083–8.
Hu Y, Mitchell KM, Albahadily FN, Michaelis EK, Wilson GS. Direct measurement of glutamate release in the brain using a dual enzyme-based electrochemical sensor. Brain Res 1994;659:117–25.
Hume RI, Role LW, Fischbach GD. Acetylcholine release from growth cones detected with patches of acetylcholine receptor-rich membranes. Nature 1983;305:632–4.
Jabaudon D, Shimoto K, Yasuda-Kamatani Y, Scanziani M, Gahwiler BH, Gerber U. Inhibition of uptake unmasks rapid extracellular turnover of glutamate of nonvesicular origin. Proc Natl Acad Sci U S A 1999;96:8733–8.
Jaffe LF, Nuccitelli R. An ultrasensitive vibrating probe for measuring steady extracellular currents. J Cell Biol 1974;63:614–28.

Jedlicka SS, Little KM, Nivens DE, Zemlyanovdf D, Rickus JL. Peptide ormosils as cellular substrates. J Mater Chem 2007;17:5058–67.
Jedlicka SS, Dadarlat M, Hassell T, Lin Y, Young A, Zhang M, et al. Calibration of neurotransmitter release from neural cells for therapeutic implants. Int J Neural Syst 2009;19:197–212.
Jones-Villeneuve EMV, McBurney MW, Rogers KA, Kalnins VI. Retinoic acid induces embryonal carcinoma cells to differentiate into neurons and glial cells. J Cell Biol 1982;94:253–62.
Jones-Villeneuve EMV, Rundnicki MA, Harris JF, McBurney MW. Retinoic acid-induced neural differentiation of embryonal carcinoma cells. Mol Biol Cell 1983;3:2271–9.
Kauffman JM. Biosensors: unique tools in pharmaceutical and biomedical sciences. J Pharm Sci 2003;28:107–12.
Kaupmann K, Huggel K, Heid J, Flor PJ, Bischoff S, Mickel SJ, et al. Expression cloning of GABA(B) receptors uncovers similarity to metabotropic glutamate receptors. Nature 1997;386(6622):239–46.
Krivoy A, Fischel T, Weizman A. The possible involvement of metabotropic glutamate receptors in schizophrenia. Eur Neuropsychopharm 2008;18(6):395–405.
Kühtreiber WM, Jaffe LF. Detection of extracellular calcium gradients with a calcium-specific vibrating electrode. J Cell Biol 1990;110:1565–73.
Kunkel JG, Cordeiro S, Xu Y, Shipley AM, Feijó JA.Volkov AG, editor. Plant electrophysiology: theory and methods. Berlin: Springer; 2006. p. 109–37, chapter 5.
Land SC, Porterfield DM, Sanger RH, Smith PJS. The self-referencing oxygen-selective microelectrode: detection of transmembrane oxygen flux from single cells. J Exp Biol 1999;202:211–8.
Matute C, Alberdi E, Domercq M, Sanchez-Gomez MV, Perez-Samartin A, Rodriguez-Antiguedad A, et al. Excitotoxic damage to white matter. J Anat 2007;210:693–702.
McBurney MW, Rogers BJ. Isolation of male embryonal carcinoma cells and their chromosome replication patterns. Dev Biol 1982;89:503–8.
McLamore ES, Porterfield DM, Banks MK. Non invasive self-referencing electrochemical sensors for quantifying real time biophysical flux in biofilms. Biotechnol Bioeng 2009;102:791–9.
Mueller HT, Haroutunian V, Davis KL, Meador-Woodruff JH. Expression of the ionotropic glutamate receptor subunits and NMDA receptor-associated intracellular proteins in the substantia nigra in schizophrenia. Mol Brain Res 2004;121(1–2):60–9.
Nakanishi S. Molecular diversity of glutamate receptors and implications for brain function. Science 1992;258(5082):597–603.
Nedergaard M, Takano T, Hansen AJ. Beyond the role of glutamate as a neurotransmitter. Nat Rev Neurol 2002;3:748–55.
Ni YC, Púrpura V. Dual regulation of Ca^{2+}-dependent glutamate release from astrocytes: vesicular glutamate transporters and cytosolic glutamate levels. Glia 2009;57(12):1296–305.
Ni Y, Malarkey EB, Parpura V. Vesicular release of glutamate mediates bidirectional signaling between astrocytes and neurons. J Neurochem 2007;103:1273–84.
Niwa O, Horiuchi T, Torimitsu K. Continuous monitoring of L-glutamate released from cultured nerve cells by an online sensor coupled with microcapillary sampling. Biosens Bioelectron 1997;12(4):311–9.
Oldenziel WH, van der Zeyden M, Dijkstra G, Ghijsen WEJM, Karst H, Cremers TIHF, et al. Monitoring extracellular glutamate in hippocampal slices with a microsensor. J Neurosci Methods 2007;160:37–44.
Ouyang CH, Guo LJ, Lu Q, Xu XL, Wang HX. Enhanced activity of GABA receptors inhibits glutamate release induced by focal cerebral ischemia in rat striatum. Neurosci Lett 2007;420(2):174–8.
Perea G, Araque A. Astrocytes potentiate transmitter release at single hippocampal synapses. 317;2007:1083-1086.
Perea G, Navarrete M, Araque A. Tripartite synapses: astrocytes process and control synaptic information. Trends Neurosci 2009;32:421–31.
Pin JP, Duvoisin R. Review: neurotransmitter receptors. I. The metabotropic glutamate receptors: structure and functions. Neuropharmacology 1995;34(1):1–26.
Porterfield DM. Measuring metabolism and biophysical flux in the tissue, cellular and sub-cellular domains: recent developments in self-referencing amperometry for physiological sensing. Biosens Bioelectron 2007;22:1086–96.
Porterfield DM, Trimarchi JR, Keefe DL, Smith PJS. Characterization of oxygen and calcium fluxes from early mouse embryos and oocytes. Biol Bull 1998;195(2):208–9.
Rickus JL, Tobin AJ, Zink JI, Dunn B. Photochemical enzyme co-factor regeneration: towards continuous glutamate monitoring with a sol–gel optical biosensor. Mater Res Soc Symp Proc 2001;662:155–61.
Rossi DJ, Oshima T, Attwel D. Glutamate release in severe brain ischaemia is mainly by reversed uptake. Nature 2000;403:316–21.
Sanchez BC, Ochoa-Acuña H, Porterfield DM, Sepúlveda MS. Oxygen flux as an indicator of physiological stress in fathead minnow (*Pimephales promelas*) embryos: a real time biomonitoring system of water quality. Environ Sci Technol 2008;42:7010–7.
Schmitz Y, Luccarelli J, Kim M, Wang M, Sulzer D. Glutamate controls growth rate and branching of dopaminergic axons. J Neurosci 2009;29(38):11973–81.
Shimamoto K, Lebrun B, Yasuda-Kamatani Y, Sakaitani M, Shigeri Y, Yumoto N, et al. DL-threo-beta-benzyloxyaspartate, a potent blocker of excitatory amino acid transporters. Mol Pharmacol 1998;53:195–201.
Staats KA, van Den Bosch L. Astrocytes in amyotrophic lateral sclerosis: direct effects on motor neuron survival. J Bio Phys 2009;35(4):337–46.
Tabuchi A, Oh E, Taoka A, Sakurai H, Tsuchiya T, Tsuda M. Rapid attenuation of AP-1 posttranscriptional factors associated with nitric oxide-mediated neuronal cell death. J Biol Chem 1996;271:31061–7.
Takano T, Kang J, Jaiswal JK, Simon SM, Lin JHC, Yu YF, et al. Receptor-mediated glutamate release from volume sensitive channels in astrocytes. Proc Natl Acad Sci U S A 2005;102(45):16466–71.
Tapiero H, Mathe G, Couvreur P, Tew KD. Glutamine and glutamate. Biomed Pharmacother 2002;56:446–57.
ul Haque A, Chatni MR, Li G, Porterfield DM. Biochips and other microtechnologies for physiomics. Expert Rev Proteomics 2007;4:553–63.
Waagepetersen HS, Shimamoto K, Schousboe A. Comparison of effects of DL-threo-beta-benzyloxyaspartate (dl-TBOA) and L-trans-pyrrolidine-2,4-dicarboxylate (t-2,4-PDC) on uptake and release of D-aspartate in astrocytes and glutamatergic neurons. Neurochem Res 2001;26:661–6.
Wang J, Musameh M, Lin Y. Solubilization of carbon nanotubes by Nafion toward the preparation of amperometric biosensors. J Am Chem Soc 2003;125(9):2408–9.
Watson CJ, Venton BJ, Kennedy RT. In vivo measurements of neurotransmitters by microdialysis sampling. Anal Chem 2006;78:1391–9.
Wilson GS, Gifford R. Biosensors for real time in vivo measurements. Biosens Bioelectron 2005;20:2388–403.
Wu AG, Fujikawa DG. Effects of AMPA-receptor and voltage-sensitive sodium channel blockade on high potassium-induced glutamate release and neuronal death in vivo. Brain Res 2002;946(1):119–29.
Ye ZC, Rothstein JD, Sontheimer H. Compromised glutamate transport in human glioma cells: reduction-mislocalization of sodium-dependent glutamate transporters and enhanced activity of cystine–glutamate exchange. J Neurosci 1999;19(24):10767–77.
Ye ZC, Wyeth MS, Baltan-Tekkok S, Ransom BR. Functional hemichannels in astrocytes: a novel mechanism of glutamate release. J Neurosci 2003;23(9):3588–96.
Zhang S, Takeda Y, Hagioka S, Takata K, Aoe H, Nakatsuka H, et al. Brain Res Brain Res Protoc 2005;14(2):61–6.
Zuberi M, Liu-Snyder P, Ul Haque A, Porterfield DM, Borgens RB. Large naturally-produced electric currents and voltage traverse damaged mammalian spinal cord. J Biol Eng 2008;30:2–17.